Complete fusion of $^{16,18}O$ with $^{24,26}Mg$

S. L. Tabor,* D. F. Geesaman, W. Henning, D. G. Kovar, and K. E. Rehm†
Argonne National Laboratory, Argonne, Illinois 60439‡

F. W. Prosser, Jr.
University of Kansas, Lawrence, Kansas 66045

(Received 9 January 1978)

Total fusion cross sections for $^{16}O+^{24}Mg$, $^{16}O+^{26}Mg$, and $^{18}O+^{24}Mg$ have been measured in the energy range 18 MeV $\leq E_{c.m.} \leq$ 50 MeV by detection of the evaporation residues. In addition, elastic scattering angular distributions have been measured and analyzed with the optical model. The fusion cross section for $^{16}O+^{24}Mg$ saturates at $\sim$1100 mb, while that for $^{16}O+^{26}Mg$ and $^{18}O+^{24}Mg$ reaches $\sim$1200 mb. The fusion cross section excitation functions can be well described by the model of Glas and Mosel using reasonable parameters; the model of Bass reproduces the data well above $E_{c.m.} \approx 25$ MeV but overpredicts the cross section below this energy.

[NUCLEAR REACTIONS $^{16}O+^{24}Mg$, $E_{lab}=30-81$ MeV; $^{16}O+^{26}Mg$, $E_{lab}=29.4-81$ MeV; $^{18}O+^{24}Mg$, $E_{lab}=32-72$ MeV; measured σ_{fusion}; measured $\sigma(\theta)$ elastic scattering; deduced optical-model parameters.]

I. INTRODUCTION

The systematics of heavy-ion-induced fusion reactions exhibit a number of interesting characteristics which deserve further experimental investigation. We have undertaken a study of $^{16,18}O+^{24,26}Mg$ complete fusion reactions because these systems provide tests for several possible generalizations about the behavior of the heavy-ion fusion process.

Pronounced oscillations have been observed[1-5] in the fusion cross sections (σ_{fus}) for the $^{12}C+^{12}C$, $^{12}C+^{16}O$, and $^{16}O+^{16}O$ reactions as a function of incident energy. $^{16}O+^{24}Mg$ is another member of this sequence of systems, whose mass and charge numbers are multiples of those of the α particle. The determination of whether structure is present in $\sigma_{fus}(E)$ for the $^{16}O+^{24}Mg$ system indicates how widespread this phenomenon is and aids in understanding the nature of the process.

The maximum fusion cross section, σ_{fus}^{max}, observed for the $^{12}C+^{12}C$, $^{12}C+^{14}N$, and $^{12}C+^{16}O$ systems is $\approx$950 mb (Refs. 1, 2, and 6) while that for many other systems[2,7] including $^{12}C+^{18}O$, $^{12}C+^{19}F$, and $^{16}O+^{40}Ca$ lies between 1100 and 1200 mb. Although there is one counterexample[8,9] (i.e., $^{12}C+^{15}N$) to the interpretation of this difference as a shell effect,[2] the maximum fusion cross section for targets near the middle of the $2s$-$1d$ shell (such as Mg) is of interest. Since the magnitude and shape of $\sigma_{fus}(E)$ are so different[2] for the $^{12}C+^{16}O$, and $^{12}C+^{18}O$ reactions, it is of interest to determine what differences in σ_{fus} exist between the $^{16}O+^{24}Mg$ and $^{18}O+^{24}Mg$ reactions. Furthermore, a comparison with the $^{16}O+^{26}Mg$ reaction provides a test of isotopic differences not involving a shell crossing.

Another aspect of nuclear structure which motivated the study of the $^{16}O+^{24}Mg$ reaction is the large deformation[10] ($\delta=0.40$) and strong collectivity of ^{24}Mg, which could potentially influence σ_{fus} in two ways: (1) Increasing deformation increases the size of the low-density nuclear surface where low-energy heavy-ion reactions take place. This could increase the critical radius[11] for fusion and lead to a larger fusion cross section. (2) A strong coupling to the collective degrees of freedom may provide a more efficient mechanism for transfer of kinetic energy to internal excitation and influence σ_{fus}. It is possible that the very large value of σ_{fus} (i.e., 1470 $\pm$ 200 mb) reported[12] for the $^{12}C+^{20}Ne$ reaction is evidence for such an effect, since ^{20}Ne is also very deformed and collective. The $^{16}O+^{24}Mg$ fusion reaction provides a test of this hypothesis.

The fusion cross sections for the reactions $^{16}O+^{24}Mg$, $^{16}O+^{26}Mg$, and $^{18}O+^{24}Mg$ have been measured at a number of laboratory energies between 30 and 81 MeV. The fusion products were identified by their differential energy loss in a gas-ionization counter and all particles with $Z \geq 14$ were counted as evaporation residues. Symmetric fission is not expected to compete with particle evaporation from the compound system for these light systems and no evidence for fission products was seen.

II. EXPERIMENTAL TECHNIQUE

Self-supporting ^{24}Mg and ^{26}Mg targets of $\approx$200 $\mu g/cm^2$ areal density were used in the measure-

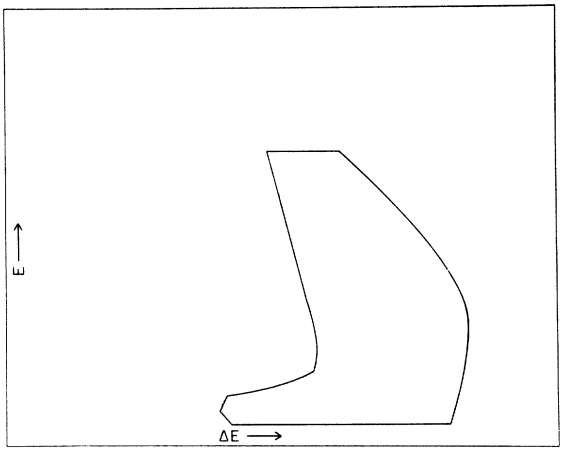

FIG. 1. Contour plot of the $\Delta E - E$ counter telescope data for $^{16}O + ^{24}Mg$ at 72 MeV incident energy at $\theta_{lab} = 6°$. The evaporation residues are encircled.

ments. The position and angle of the ^{16}O and ^{18}O beams on target were held constant by the tight collimation system of the Argonne 60-in. scattering chamber. Forward-angle elastic-scattering measurements on both sides of the beam were used to determine the 0° position of each detector arm to $\leq 0.02°$.

Very little oxygen contamination was observed on the targets. During most of the measurements the target was surrounded by a liquid-nitrogen-chilled shroud which virtually eliminated carbon buildup. When the cold trap was not in use, a fresh target was substituted whenever appreciable carbon buildup was observed in the monitor spectra.

A system of 3 surface-barrier detectors was used to monitor the beam intensity in addition to the current integrator. Detectors were placed on each side of the beam at $\theta = 10°$ to monitor any beam shift as well as the product of target thickness times beam flux. When the cold shroud was not used, this detector pair was raised about 10° above beam height to avoid being blocked by other detectors. It was necessary to place all detectors at the beam height when using the target shroud. The third monitor detector was located on the opposite side of the beam from the counter telescope at angles of 15° to 20°. It was also used in measurements of elastic scattering angular distributions.

Evaporation residues were detected with a counter telescope using a gas-ionization ΔE counter, similar to that described by Fowler and Jared,[13] and a conventional silicon surface-barrier E detector. The E detector was placed within the gas volume so that only one window (~50 μg/cm^2 of VYNS) was used. The gas thickness (10% CH_4 and 90% Ar) was ~300 μg/cm^2.

An example of the particle identification obtained from this telescope is shown in Fig. 1; ΔE pulse height is displayed along the x axis and the remaining energy, E, along the y axis. The data were stored as a 128×256 channel array in the PDP-11 memory. The region in ΔE-E space outlined in Fig. 1 was integrated to determine the yield of fusion products. It extends from $Z = 14$ to 20. Identification of the fusion products poses no difficulty if the target is free of contaminants, except at very low energies where the evaporation residues merge with the oxygen group. However, there is not much fusion yield in the region of overlap and it represents a small uncertainty which amounts to about 5% in the most unfavorable cases at low bombarding energies.

III. ELASTIC SCATTERING

The elastic^{16,18} O yield was measured simultaneously with that of the evaporation residues in the gas-counter telescope. In several cases elastic-scattering angular distributions were also measured with the movable monitor detector. Examples of the angular distributions are shown in Fig. 2.

Optical-model (OM) analyses of the elastic-scattering data were performed to determine total re-

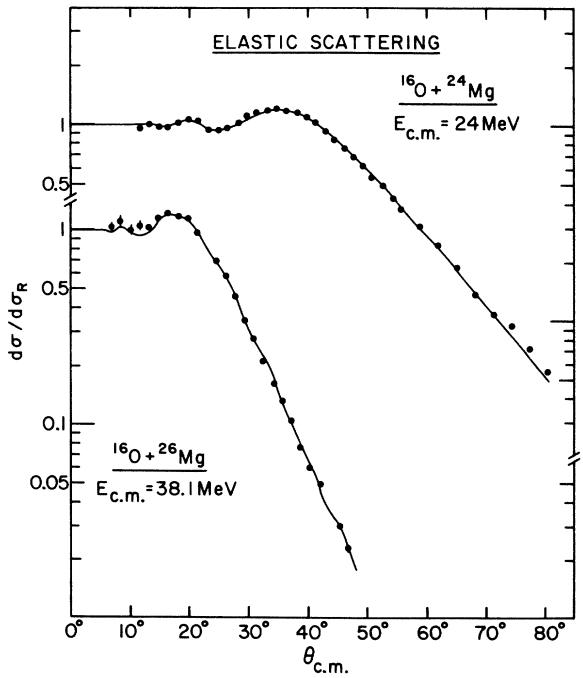

FIG. 2. Elastic scattering angular distributions. Uncertainties are smaller than the dots except where indicated. The solid lines are optical-model fits.

TABLE I. Energy-independent optical-model parameters as obtained in a fit to elastic scattering data at 4 energies between 32 MeV $\leq E_{lab} \leq$ 72 MeV. Four parameters (r_{0r}, a_r, r_{0I}, a_I) were varied; the potential depths V_0 and W_0 were kept constant. The nuclear optical potential is given by

$$V(r) = \frac{V_0}{\{1+\exp[(r-R_r)/a_r]\}} + \frac{iW_0}{\{1+\exp[(r-R_I)/a_I]\}}$$

with $R_r = r_{0r}(A_1^{1/3}+A_2^{1/3})$ $R_I = r_{0I}(A_1^{1/3}+A_2^{1/3})$.

System	V_0 (MeV)	r_{0r} (fm)	a_r (fm)	W_0 (MeV)	r_{I0} (fm)	a_I (fm)
$^{16}O+^{24}Mg$	10	1.452	0.345	23	1.272	0.376
$^{16}O+^{26}Mg$	10	1.390	0.473	23	1.200	0.528
$^{18}O+^{24}Mg$	10	1.421	0.356	23	1.200	0.524
$^{16}O+^{28}Si$ [a]	10	1.350	0.618	23.4	1.230	0.552

[a] Reference 15.

action cross sections and were used to normalize the fusion data. For each of the three systems studied, elastic angular distributions at 4 different incident energies were fitted using the heavy-ion program, PTOLEMY, of Gloeckner, Macfarlane, and Pieper.[14] All 4 energies were fitted simultaneously.

As starting parameters we took those of the energy-independent potential of Cramer *et al.*,[15] which describes $^{16}O+^{28}Si$ elastic scattering over a large range of energies, including the center-of-mass (c.m.) energy range of the systems studied here. Following the authors of Ref. 15, the real and imaginary potential depths were fixed at values of $V_0 = 10$ MeV and $W_0 = 23$ and only the geometry of the potentials was allowed to vary. The potential parameters obtained in the fits are listed in Table I. Some sample comparisons of the optical-model fits with the data are shown in Fig. 2. To test how well the total reaction cross section (σ_R) is determined by the data, independent 6-parameter fits were also made at each energy. The differences in σ_R indicate that its uncertainty could be as high as ±10%.

IV. FUSION CROSS SECTIONS

All particles observed in the counter telescope with $14 \leq Z \leq 20$ were treated as evaporation residues. No evidence for fission products ($Z \sim 10$) was observed, so the evaporation residue yields were taken as a measure of the complete fusion yields. Several precautions were taken to ensure that essentially all the evaporation residues were detected. Particles which enter the detector telescope but fail to reach the E detector because of multiple scattering in the gas volume will lie along the x axis of Fig. 1. Only a small number of such

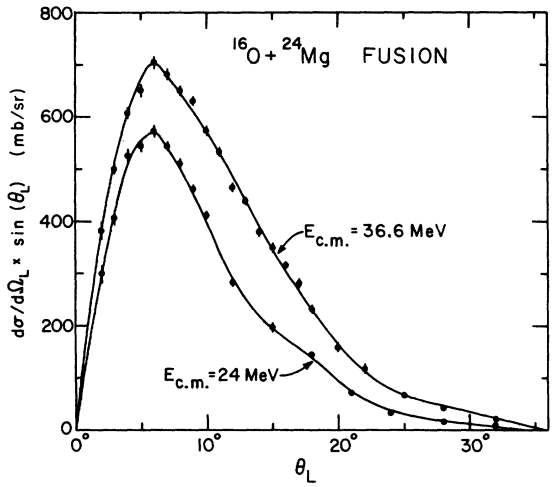

FIG. 3. Angular distributions of the $^{16}O+^{24}Mg$ fusion cross sections at the indicated incident energies. $(d\sigma/d\Omega)\sin\theta$ is graphed so that the area under the curves is the angle-integrated cross section.

events was observed, but the acceptance windows were drawn to include them. As was mentioned previously, the number of very low energy residues which cannot be distinguished from low energy ^{16}O particles is estimated to be less than 5%. Further testing was made at low bombarding energies where the residues have low recoil velocities and are most difficult to detect. The yield of eveporation residues was observed to remain constant when the gas pressure in the chamber (and hence ΔE detector thickness) was varied over a range from $\frac{1}{2}$ to twice the normal value.

Angular distributions of the evaporation residue yields were measured in order to determine the total fusion cross section. The relative normalization for the angular distribution measurements was

TABLE II. Cross sections for the complete fusion of ^{16}O and ^{24}Mg.

$E_{c.m.}$	σ_{fus} (mb)
18.0	258 ± 18
19.5	411 ± 29
21.6	613 ± 40
24.0	754 ± 30
26.4	885 ± 54
28.8	972 ± 39
31.2	1037 ± 62
33.6	1036 ± 41
36.6	1070 ± 43
39.6	1074 ± 65
43.2	1101 ± 44
48.6	1116 ± 45

TABLE III. Cross sections for the complete fusion of ^{16}O and ^{26}Mg.

$E_{c.m.}$	σ_{fus} (mb)
18.2	221 ± 20
20.0	416 ± 29
22.2	603 ± 48
25.0	817 ± 33
26.7	910 ± 55
28.6	971 ± 58
30.8	1 052 ± 63
33.3	1 124 ± 67
36.4	1 148 ± 69
38.1	1 181 ± 47
40.0	1 177 ± 71
44.5	1 196 ± 48
50.1	1 177 ± 50

TABLE IV. Cross sections for the complete fusion of ^{18}O and ^{24}Mg.

$E_{c.m.}$	σ_{fus} (mb)
18.3	386 ± 39
20.0	468 ± 37
22.9	665 ± 27
25.7	813 ± 49
28.6	920 ± 55
31.4	1 058 ± 63
34.3	1 090 ± 65
36.0	1 137 ± 45
38.3	1 179 ± 71
41.1	1 210 ± 48

provided by the monitor detectors. The yield of elastically scattered ions detected simultaneously with the evaporation residues was used to establish the absolute normalization of σ_{fus}. Since the uncertainty in the elastic scattering cross section due to beam shifts and to other effects increases rapidly at forward angles, generally only the elastic scattering data at angles greater than 6° were used for normalization. At lower energies, there is a significant angular region beyond 6° where σ_{el} is equal to the Rutherford cross section, which is convenient for normalization. At higher energies σ_{el} was compared to OM predictions over a range of angles for normalization. Uncertainty in determination of the absolute normalization appears to be the largest contribution to the uncertainty in σ_{fus}.

In Fig. 3 some examples of the angular distributions observed for the evaporation residues are shown. Measurements were made as far forward

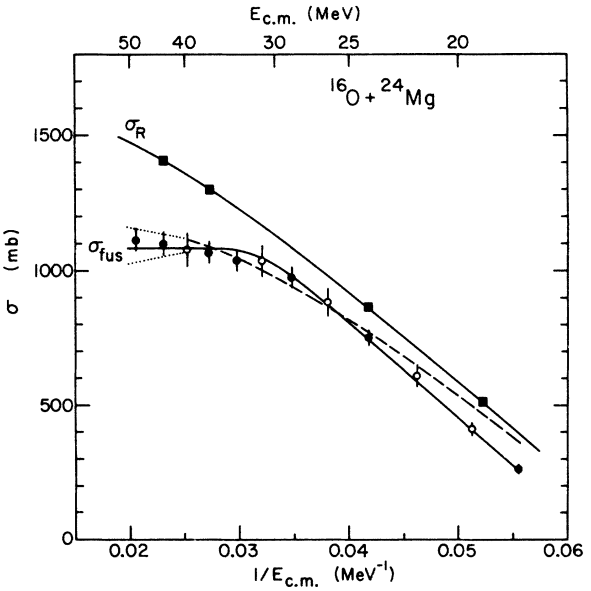

FIG. 4. The $^{16}O + ^{24}Mg$ fusion cross section as a function of inverse center-of-mass energy. The solid circles are the values of σ_{fus} obtained from angular distributions while the single angle points are plotted as open circles. The solid line through the σ_{fus} points is a fit obtained from the model of Glas and Mosel (Ref. 11). The dashed line and the 2 dotted lines represent predictions from the model of Bass (Ref. 23). The squares indicate the energies at which optical-model fits were made to the elastic scattering data and the line through these squares represents the OM total reaction cross section.

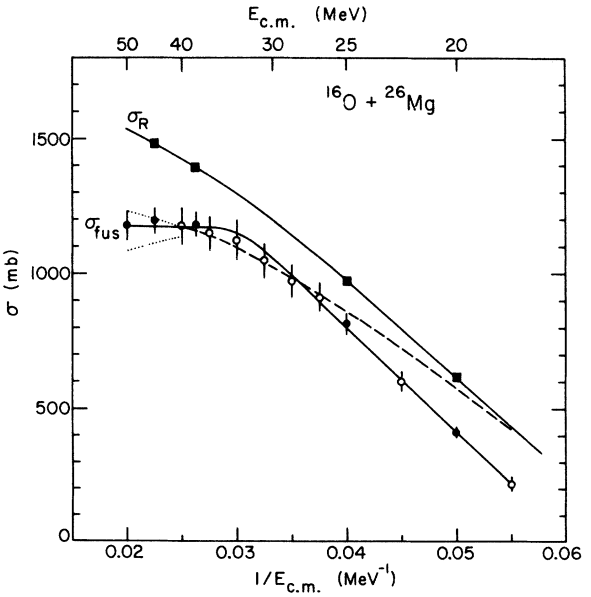

FIG. 5. Fusion and total reaction cross sections for the $^{16}O + ^{26}Mg$ reaction. Details of the figure are the same as those discussed in the caption of Fig. 4.

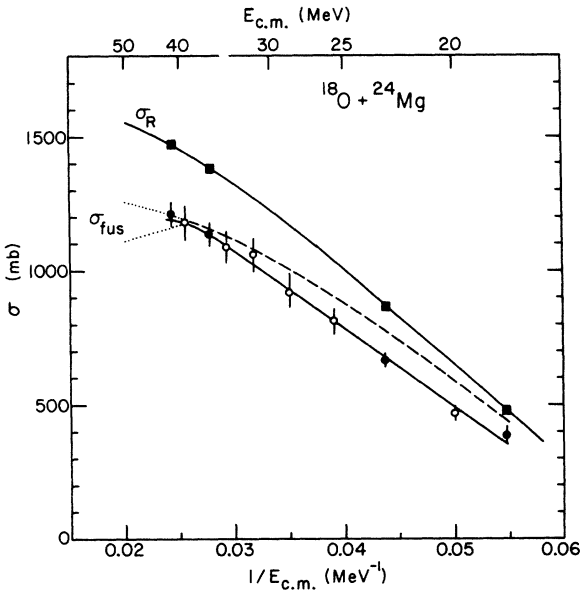

FIG. 6. Fusion and total reaction cross sections for the $^{18}O+^{24}Mg$ reaction. Details of the figure are the same as those discussed in the caption of Fig. 4.

as 2° in most cases. σ_{fus} was determined by numerically integrating these angular distributions. It can be seen in Fig. 3 that the shape of the angular distributions changes rather slowly with beam energy. Consequently, excitation curves at $\theta_{lab} = 6°$ (the approximate peak of $d\sigma_{fus}/d\theta$) were measured to supplement the angular distribution measurements. The conversion of $d\sigma_{fus}(6°)/d\Omega$ to σ_{fus} was interpolated between the energies at which angular distributions were measured. As a result, the single angle points are estimated to have a somewhat higher uncertainty. The resulting fusion cross sections are listed in Tables II, III, and IV and are graphed in Figs. 4–6 for the three systems studied. In these figures σ_{fus} is shown as a function of $1/E_{c.m.}$ to facilitate comparison with models to be discussed later. Also plotted in Figs. 4–6 are the total reaction cross sections predicted by the optical-model parameters of Table I.

V. DISCUSSION

A. Phenomenology

Several noteworthy features of the fusion data are apparent in Figs. 4–6:

(1) σ_{fus} reaches maximum values of 1100 to 1200 mb for the $^{16,18}O+^{24}Mg$ and $^{16}O+^{26}Mg$ systems. These values are comparable to the maximum fusion cross sections observed for other systems involving $2s$-$1d$ nuclei, including the $^{18}O+^{12}C$ (Ref. 2), $^{12}C+^{27}Al$ (Ref. 16), $^{16}O+^{27}Al$ (Refs. 17, 18), and $^{16}O+^{40}Ca$ (Ref. 7) reactions, but are significantly smaller than the value reported[12] for the $^{12}C+^{20}Ne$ system. Hence the deformed, collective nature of ^{24}Mg apparently does not strongly affect the maximum fusion cross section and suggests that deformation is not the cause of the large value of σ_{fus} observed for the $^{12}C+^{20}Ne$ system.

(2) There is no evidence for oscillations in $\sigma_{fus}(E)$ for $^{16}O+^{24}Mg$ with amplitude >5%. The combinations of ^{12}C and ^{16}O remain the only colliding systems known to exhibit oscillatory fusion cross sections. Since $\sigma_{fus}(E)$ oscillates for $^{16}O+^{16}O$ but not for $^{16}O+^{24}Mg$, it would now be very interesting to investigate $^{16}O+^{20}Ne$ which lies between these systems.

(3) The fusion cross sections for $^{16}O+^{24}Mg$ and $^{16}O+^{26}Mg$ rise parallel to the total reaction cross section σ_R with increasing incident energy up to about 30 MeV and then saturate. σ_{fus} exhausts a large fraction of σ_R below 30 MeV. $\sigma_{fus}(E)$ for $^{18}O+^{24}Mg$ rises less rapidly than σ_R and the data do not extend to high enough energies to verify whether σ_{fus} has reached saturation.

The fusion cross section behavior for these systems is compared in Fig. 7. With the exception of the lowest energy $^{18}O+^{24}Mg$ point, σ_{fus} is identical within errors for all 3 systems up to ~30 MeV. Above 30 MeV the fusion cross sections for the $^{16}O+^{26}Mg$ and $^{18}O+^{24}Mg$ systems continue to rise together until the data for ^{18}O ends, while σ_{fus} for $^{16}O+^{24}Mg$ remains somewhat lower. As a result, the systems with a neutron excess reach a maximum fusion cross section ~100 ± 50 mb higher.

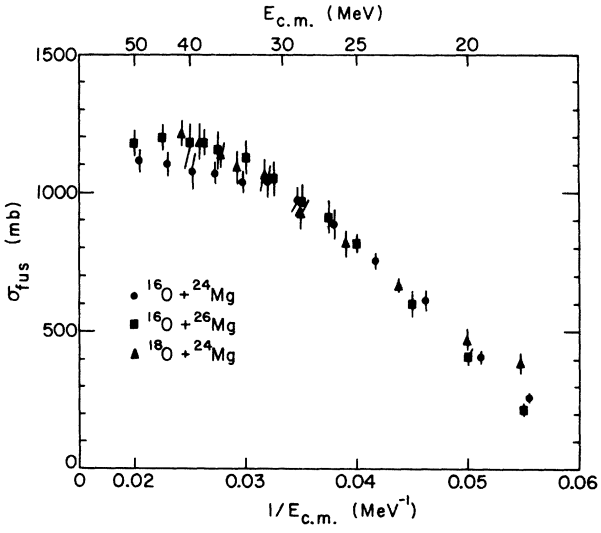

FIG. 7. A comparison of σ_{fus} for $^{16}O+^{24}Mg$, $^{16}O+^{26}Mg$, and $^{18}O+^{24}Mg$ plotted as function of inverse center-of-mass energy.

With the available data it is not possible to conclude whether σ_{fus} for $^{16}O+^{24}Mg$ and $^{16}O+^{26}Mg$ are converging at high energy or remain ~100 mb apart. Measurements at higher energies are needed to answer this question.

Eisen *et al.* have observed that σ_{fus} at constant $E_{c.m.}$ increases with projectile mass in the $^{16,17,18}O+^{27}Al$ systems.[19] The $^{18}O-^{16}O$ difference is ~70 ± 40 mb in the 17–26-MeV energy range which they studied. Such a difference is not seen for $^{16,18}O+^{24}Mg$ except possibly below 20 MeV.

B. Glas-Mosel model

The model of Glas and Mosel[11] assumes that the colliding ions must reach a certain critical distance R_C before fusion can occur. At high incident energies their expression for the fusion cross section becomes approximately

$$\sigma_{fus}(E)=\pi R^2[1-V(R)/E], \quad (1)$$

where $R=R_C$ ("critical" radius). At low energies fusion is limited by the interaction barrier, which Glas and Mosel treat in a parabolic barrier approximation. Their formula also reduces to Eq. (1) at low energies with $R=R_B$, the interaction barrier radius. The model has 5 parameters: the two radii R_C and R_B, the real nuclear plus Coulomb ion-ion potentials at those points $V(R_C)$ and $V(R_B)$, and a barrier width parameter $\hbar\omega$.

One approach to the comparison of model and data is to search for the parameters which yield optimum fits to each data set individually. The stability and trends of the derived parameters then serve to define the applicability of the model. Because the present data are not sufficient to determine 5 parameters, we have fixed 2 parameters in the Glas-Mosel formula and allowed the other 3 to vary. The barrier width $\hbar\omega$ was fixed at 5 MeV and $V(R_C)$, the slope of the high-energy curve, was fixed at 0 MeV, corresponding to a constant $\sigma_{fus}(E)$ for large E.

The resulting Glas-Mosel fits are shown in Figs. 4–6 and the parameters are listed in Table V. It is obvious that the fits are excellent, indicating that the data are at least consistent with the model. It might be argued that the $^{16}O+^{24}Mg$ data imply a slowly rising σ_{fus} at high energy, but the data are also completely consistent with the assumption of constant σ_{fus}. Measurements at higher energies are needed to determine $V(R_C)$. In fact, the $^{18}O+^{24}Mg$ data do not extend beyond the region dominated by the interaction barrier. Recent measurements[20] of the $^{16}O+^{26}Mg$ reaction at higher energies indicate that $\sigma_{fus}(E)$ remains constant or decreases slightly with increasing energy in the region 40 MeV $\leq E_{c.m.} \leq$ 70 MeV.

TABLE V. A comparison of Glas-Mosel parameters for the present data with those of other light systems. The error bars for $r_B(R_B)$ and V_B are approximately ±3% for our data; for the systems quoted from literature the uncertainties range from 1 to 3%. Since V_C was set to a fixed value due to the lack of high-energy data in most cases, no meaningful error bars can be extracted for V_C and consequently for $r_C(R_C)$: $R_{B,C}=r_{B,C}(A_1^{1/3}+A_2^{1/3})$.

System	r_B (fm)	R_B (fm)	V_B (MeV)	r_C (fm)	R_C (fm)	V_C (MeV)
$^{18}O+^{12}C$ [a]	1.60	7.86	7.5	1.04	5.11	−10
$^{19}F+^{12}C$ [a]	1.54	7.64	8.1	1.03	5.11	−10
$^{16}O+^{24}Mg$	1.57	8.48	16.0	1.08	5.84	0
$^{16}O+^{26}Mg$	1.59	8.72	16.6	1.12	6.14	0
$^{18}O+^{24}Mg$	1.42	7.82	14.8	1.15	6.33	0
$^{16}O+^{27}Al$ [b]	1.44	7.95	16.1	0.79	4.36	−46.3
[c]	1.48	8.19	15.7	...	...	...
$^{16}O+^{40}Ca$ [d]	1.46	8.67	22.6	1.02	6.06	0
$^{32}S+^{24}Mg$ [e]	1.44	8.72	28.3	0.97	5.88	0

[a] Reference 2.
[b] Reference 18.
[c] Reference 19.
[d] Reference 7.
[e] Reference 25.

Included in Table V for comparison are Glas-Mosel parameters for a number of lighter and heavier systems.[2,7,18,19,25] It can be seen that the parameters vary rather consistently although fluctuations as large as 10% can be noted. As expected, the interaction barrier height V_B increases considerably with Z_1Z_2 while the reduced barrier r_B decreases slowly. More interesting is that the reduced critical radius for fusion, r_C, remains constant within 10% over the rather wide range of colliding systems except for $^{16}O+^{27}Al$.[18] However, as pointed out in Ref. 18, the values of $r_C(R_C)$ and V_C have large error bars due to systematic uncertainties in the original data. Since simple size effects are accounted for through the reduced radii, the fact that r_C does not change significantly suggests that the critical distance for fusion depends on a critical nuclear density overlap.

C. Bass model

In a recent letter,[21] Bass presented a classical analysis of fusion cross section data in which an empirical nucleus-nucleus potential was extracted. In this analysis it was assumed that the fusion cross section is given by the well-known relationship,

$$\sigma_{fus}(E)=\pi r_{fus}^2\left[1-\frac{V(r_{fus})}{E}\right].$$

At low bombarding energies r_{fus} is the radius of the interaction barrier which must be overcome in order to reach the radius, R_C, where fusion occurs.[11,21-23] Specifically, r_{fus} is taken to be the

classical turning point of the limiting trajectory; i.e., r_{fus} which in general depends on energy is defined by the condition that the quantity $r^2[E - V(r)]$ is minimized for some $r \geq R_C$. At higher bombarding energies, where the centrifugal plus Coulomb potentials for the largest partial waves prevent the two nuclei from reaching R_C, the value for r_{fus} is taken to be equal to R_C. In Bass's analysis corresponding pairs r_{fus}, $V(r_{fus})$ were deduced from fusion data by graphical techniques and used to establish an average nucleus-nucleus potential.

Shown in Figs. 4–6 as dashed curves are the predicted fusion cross section behaviors obtained using Bass's empirical potential. Above $E_{c.m.} = 40$ MeV the predicted fusion cross section is determined by the choice of R_C. The two dotted curves in each figure represent different choices for R_C. The upper dotted curve corresponds to R_C set equal to the value of r_{fus} obtained ($\approx$6.5–6.9 fm) at the highest bombarding energy ($E_{c.m.} \approx 40$ MeV) before the disappearance of a minimum in the quantity $r^2[E - V(r)]$. The lower dotted curve corresponds to R_C set equal to the sum of half density radii ($\approx$5.2–5.4 fm) as calculated with the parametrization given by Bass.

When comparing the Bass and Glas-Mosel curves in Figs. 4–6, it should be remembered that the latter were fitted to each data set, while the former represent a global search not including these data. It is clear that the Bass model overpredicts the fusion cross section at low energies but converges to the data at 25–30 MeV. In fact, the model predicts σ_{fus} very well at about 40 MeV and even reproduces the difference between $^{16}O + ^{24}Mg$ and the neutron-excess systems. At still higher energies it is obvious that a choice of r_{fus} between those values used to calculate the dotted lines would reproduce the data nicely.

The difference between the Bass prediction at low energies and the O + Mg data is the largest that has been observed for light systems.[24] It is not yet clear whether this discrepancy represents a weakness in the model, a difference between fusion in the present systems and the ones fit by Bass, or a region of $V(r)$ which could be adjusted to fit O + Mg without materially worsening the other fits.

VI. CONCLUSION

The general behavior of σ_{fus} for the $^{16,18}O + ^{24}Mg$ and $^{16}O + ^{26}Mg$ reactions is similar to that of most other systems between $^{18}O + ^{12}C$ and $^{16}O + ^{40}Ca$. At low energies σ_{fus} is ~70–90% of σ_R (OM) but at higher energies σ_{fus} saturates at 1100–1200 mb. σ_{fus} for $^{16}O + ^{26}Mg$ and $^{18}O + ^{24}Mg$ behaves quite similarly and rises about 100 mb higher than for $^{16}O + ^{24}Mg$ in the saturation region.

The fusion cross section for these systems is consistent with the Glas-Mosel model using reasonable parameters. The Bass model, which was fitted globally to a number of other systems, overpredicts σ_{fus} at low energies but converges to the data at higher energies. Both models have in common the concept that the ion-ion distance is the most important parameter in the fusion process. All of these classical pictures of the fusion reactions appear accurate to ±100 mb, the level at which details of nuclear structure presumably become important.

---

*Present address: Department of Physics and Astronomy, University of Maryland, College Park, Maryland 20742.

†Max Kade Fellow, on leave from Technische Hochschule München, 8046 Garching, West Germany.

‡Work performed under the auspices of the Department of Energy.

[1]P. Sperr, S. Vigdor, Y. Eisen, W. Henning, D. G. Kovar, T. R. Ophel, and B. Zeidman, Phys. Rev. Lett. 36, 405 (1976).

[2]P. Sperr, T. H. Braid, Y. Eisen, D. G. Kovar, F. W. Prosser, Jr., J. P. Schiffer, S. L. Tabor, and S. Vigdor, Phys. Rev. Lett. 37, 321 (1976).

[3]S. L. Tabor, Y. Eisen, D. G. Kovar, and Z. Vager, Phys. Rev. C 16, 673 (1977).

[4]J. J. Kolata, R. M. Freeman, F. Hass, B. Hersch, and J. Gallmann, Phys. Lett. 65B, 333 (1976).

[5]Z. E. Switkowski, H. Winkler, and P. R. Christensen, Phys. Rev. C 15, 449 (1977).

[6]R. G. Stokstad, J. Gomez del Campo, J. A. Biggerstaff, A. H. Snell, and P. H. Stelson, In Proceedings of the Symposium on Macroscopic Features of Heavy-Ion Collisions, Argonne National Laboratory, Report No. ANL/PHY-76-2, Vol. II, p. 795, 1976 (unpublished).

[7]S. E. Vigdor, in Proceedings of the Symposium on Macroscopic Features of Heavy-Ion Collisions, Argonne National Laboratory, Report No. ANL/PHY-76-2, Vol. I, p. 95, 1976 (unpublished).

[8]S. Harar, in *Proceedings of the Colloque Franco-Japonais de Spectroscopie Nucleaire et Reaction Nucleaire*, edited by Y. Shida (Institute for Nuclear Study, Tokyo, 1976), p. 191.

[9]W. Henning, D. F. Geesaman, D. G. Kovar, K. E. Rehm, J. P. Schiffer, and S. L. Tabor, Bull. Am. Phys. Soc. 22, 629 (1977).

[10]A. Bohr and B. R. Mottelson, *Nuclear Structure* (Benjamin, New York, 1975), Vol. II, p. 134.

[11]D. Glas and U. Mosel, Phys. Rev. C 10, 2620 (1977).

[12]M. Conjeaud, S. Gary, S. Harar, J. M. Loiseaux, J. Menet, and J. B. Viano, in Proceedings of the European Conference on Nuclear Physics with Heavy Ions, Caen, France, 1976 (unpublished).

[13]M. M. Fowler and R. C. Jared, Nucl. Instrum. Methods 124, 341 (1975).

[14]D. H. Gloeckner, M. H. Macfarlane, and S. C. Pieper, Argonne National Laboratory Report No. ANL-76-11,

1976, (unpublished).
[15]J. G. Cramer, R. M. DeVries, D. A. Goldberg, M. S. Zisman, and C. F. Maguire, Phys. Rev. C 14, 2158 (1976).
[16]R. R. Betts, W. A. Lanford, M. H. Mortensen, and R. L. White, in Proceedings of the Symposium on Macroscopic Features of Heavy-Ion Collisions, Argonne National Laboratory, Report No. ANL/PHY-76-2, Vol. II, p. 443, 1976 (unpublished).
[17]R. L. Kozub, N. H. Lu, J. M. Miller, D. Logan, T. W. Debiak, and L. Kowalski, Phys. Rev. C 11, 1497 (1975).
[18]B. B. Back, R. R. Betts, C. Gaarde, J. S. Larsen, E. Michelsen, and Tai Kuang-Shi, Nucl. Phys. A285, 317 (1977).
[19]Y. Eisen, I. Tserruya, Y. Eyal, Z. Fraenkel, and M. Hillman, Nucl. Phys., A291, 459 (1977).
[20]D. Horn, A. J. Ferguson, and O. Hausser, Bull. Am. Phys. Soc. 22, 1021 (1977).
[21]R. Bass, Phys. Rev. Lett. 39, 265 (1977).
[22]R. Bass, Phys. Lett. 47B, 139 (1973).
[23]R. Bass, Nucl. Phys. A231, 45 (1974).
[24]D. G. Kovar, in Proceedings of the Symposium on the Macroscopic Features of Heavy Ion Reactions and the Pre-Equilibrium Processes, Hakone, Japan, 1977 (unpublished).
[25]D. G. Kovar, P. D. Bond, C. Flaum, M. J. LeVine, and C. E. Thorn, Bull. Am. Phys. Soc. 22, 66 (1977).

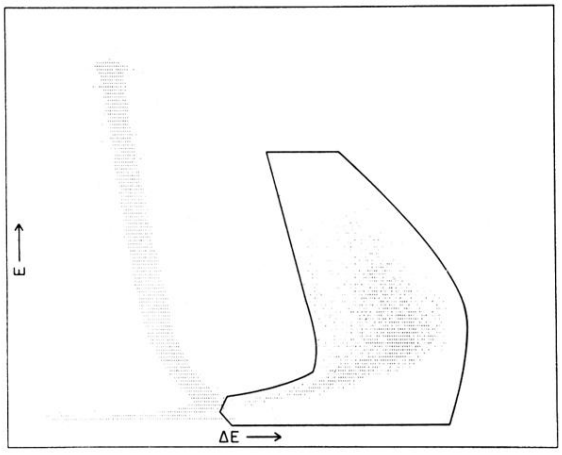

FIG. 1. Contour plot of the $\Delta E - E$ counter telescope data for $^{16}O + ^{24}Mg$ at 72 MeV incident energy at $\theta_{lab} = 6°$. The evaporation residues are encircled.